

Project 3 - FYS4150

Nanna Bryne, Johan Mylius Kroken, Vetle A. Vikenes
(Dated: October 26, 2022)

The Penning trap is a device that uses a strong axial magnetic field together with a quadrupole electric field to capture charged particles within a spatial region. We model such a trap by assuming it to be spherical, and consider an external electric and magnetic field, alongside an internal electric field set up by charged particles (Ca^+ ions) in the trap. We neglect the self induced magnetic field set up by moving charges. The equations of motion are determined by the Lorentz force, and we solve them numerically using two different integration schemes: The Forward Euler and Runge-Kutta 4 schemes. These methods offer different trade offs between computational expense and numerical accuracy, yielding a global error of $\mathcal{O}(h)$ and $\mathcal{O}(h^4)$ respectively (for step size h). We check and confirm these errors by simulating one single particle for 50 μs for different time steps using both schemes. h is small, thus the Runge-Kutta 4 scheme offers a far lower global error and is used when we make a simulation of two particles, where we also investigate the effect of the Coulomb interaction between particles. The trajectories of the particles, both in the (x, y) -plane and in the phase spaces of x and z change when we allow for particle interaction. We also explore how 100 randomly distributed particles behave under the influence of a time-dependent sinusoidal perturbation to the external electric potential. We simulate this for different amplitudes and frequencies, and find that certain resonance frequencies of this perturbation has the ability to completely empty the trap. These simulations are computationally very expensive and lengthy. However, we obtain results indicating that the simulation becomes unstable for applied frequencies of $\omega_V \in \{0.7, 1.4, 2.2\}$ MHz. For a larger applied amplitude f , we see broader resonance lines centred around these resonance frequencies. Including Coulomb interactions result in more chaotic and unstable behaviour. The code is found in the following GitHub repository: <https://github.com/Vikenes/FYS4150/tree/main/project3>.

I. INTRODUCTION

Trapping charged particles is a common and useful method in order to perform various measurements and experiments. A natural starting point would be to create a three-dimensional electric potential which pulls the particles towards a center. According to Earnshaw's theorem [3], keeping a charged particle in stable equilibrium with an electrostatic force alone is not possible. One way around this is to use a strong homogeneous axial magnetic field together with a quadrupole electric field. The former incarcerates the particle(s) radially, whereas the latter confines the particle(s) radially. A device of such a structure is called a "Penning trap" and was first built by Hans Georg Dehmelt under the influence of Frans Michel Penning's work [2]. The Lorentz force, \mathbf{F} , acting on a particle with charge q that is subjected to an electric field, \mathbf{E} , and a magnetic field, \mathbf{B} , is given by

$$\mathbf{F} = q\mathbf{E} + q\mathbf{v} \times \mathbf{B}, \quad (1)$$

where \mathbf{v} is the particle's velocity. Suppose the particle has mass m , then Newton's second law gives us the equation of motion for the particle:

$$\frac{d\mathbf{v}}{dt} = \frac{\mathbf{F}}{m} \Rightarrow \frac{d^2\mathbf{r}}{dt^2} = \frac{q}{m}(\mathbf{E} + \mathbf{v} \times \mathbf{B}). \quad (2)$$

The external electric field is related to the potential through $\mathbf{E} = -\nabla V$. By choosing a particular electric potential and magnetic field, we can solve equation (2) to predict the motion of a single particle inside a Penning trap.

In reality one is often concerned with storing multiple particles, not just a single one. This introduces Coulomb interactions between the particles, and the resulting equations of motion will then be much more cumbersome to tackle analytically. To study the motion of the trapped particles we will therefore resort to numerical integration methods.

Equation (2) can be split into two ordinary differential equations (ODEs) that we can solve numerically. The two methods we will consider are forward Euler (FE) and fourth order Runge-Kutta (RK4). FE requires fewer floating point operations (FLOPs) per iteration compared to RK4, but RK4 provides a much more accurate result at a given step size. By solving the equations of motion for a single particle in the Penning trap analytically we can estimate the error of the two numerical schemes. Estimating the accuracy of our solver when particle interactions are present is a difficult task in the absence of analytical expressions. The single particle case will therefore provide us with key insight to the validity of our solvers. By simulating two particles in the trap both with and without interactions, we can use the single particle results to evaluate our implementation.

When the basics of our solver have been studied we want to explore physical properties of the Penning trap. We will limit our analysis to a study of resonance phenomena in the trap. To do this we will subject the particles to a time-dependent electric potential, which oscillates at a certain applied frequency. If resonance occurs we expect that particles eventually escape the trap, when their distances from the origin exceed the extent of the trap itself. By devising a scheme to quantify the escape of particles we can find the frequencies at which resonance

occurs, and possibly relate this to the physical properties of the Penning trap. The final question we then want to answer is whether particle interactions affect the onset of resonance, and if so, how.

In this report we begin by introducing the Penning trap in section II. Here we present the setup of the trap and the resulting equations of motion for particles in the trap. We derive the analytical solutions for a single particle in section II B and describe the modifications to the equations of motion when interactions between multiple particles are included in section II C.

In section III A we present our numerical solver. We present our choice of parameters for the trap and the initial conditions for testing in sections III B and III C respectively. In section III D we present the analysis for a single particle, as well as two particles in the trap. Section III E focuses on our investigation of resonance phenomena in the trap.

The results of our investigations are presented in section IV. Finally, we discuss our results and present our conclusions in sections V and VI respectively.

II. THE PENNING TRAP

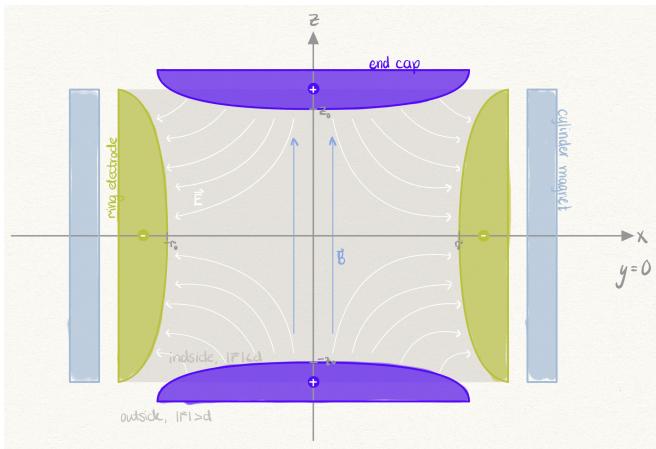


FIG. 1. Schematic of the Penning trap. The cross-section is in the xz -plane. The ring electrode (green) and end caps (dark blue) sets the inhomogeneous electric field (white arrows). The homogeneous magnetic field (blue arrows) is resulting from the cylinder magnet (light blue) outside of the trap. For simplicity, we will assume that the trap extends the distance d in all directions, see text for further details.

We consider an ideal Penning trap in three dimensions, with a schematic of the trap shown in Figure 1.

A. External electromagnetic fields

The electrodes in the Penning trap create an external electric field \mathbf{E}_{ext} defined by the potential

$$V(\mathbf{r}) = V(x, y, z) = \frac{V_0}{2d^2}(2z^2 - x^2 - y^2), \quad (3)$$

where V_0 is the potential applied to the electrodes and $d = \sqrt{z_0^2 + \frac{1}{2}r_0^2}$ is the characteristic dimension, where z_0 is the distance between the centre and the endcap and r_0 is the radius of the ring. The external electric field resulting from this potential is

$$\mathbf{E}_{\text{ext}} = -\nabla V = \frac{V_0}{d^2}(x, y, -2z), \quad (4)$$

which traps the particles in the z -direction. To contain the particles in the (x, y) -plane, a constant homogeneous magnetic field \mathbf{B}_{ext} is imposed in the z -direction,

$$\mathbf{B}_{\text{ext}} = (0, 0, B_0). \quad (5)$$

As a simplification, we consider the trap as a sphere of radius d . We set the external fields to zero outside this region, so the electric field is

$$\mathbf{E}_{\text{ext}}(\mathbf{r}) = \begin{cases} \frac{V_0}{d^2}(x, y, -2z), & |\mathbf{r}| \leq d \\ (0, 0, 0), & |\mathbf{r}| > d \end{cases}, \quad (6)$$

and the magnetic field is

$$\mathbf{B}_{\text{ext}}(\mathbf{r}) = \begin{cases} (0, 0, B_0), & |\mathbf{r}| \leq d \\ (0, 0, 0), & |\mathbf{r}| > d \end{cases}. \quad (7)$$

For the analytical derivations that follow in this section (section II), we will assume that $|\mathbf{r}| \leq d$ is fulfilled.

B. Analytical solutions - Single particle

We begin by considering a single particle in the Penning trap. The Lorentz force is then governed by the external fields only, hence $\mathbf{E} = \mathbf{E}_{\text{ext}}$ and $\mathbf{B} = \mathbf{B}_{\text{ext}}$. We use eq. (1) to compute the Lorentz force,

$$\begin{aligned} \mathbf{F} &= \frac{qV_0}{d^2}(x, y, -2z) + qB_0(y, -\dot{x}, 0) \\ &= \frac{m}{2}\omega_z^2(x, y, -2z) + m\omega_0(y, -\dot{x}, 0), \end{aligned} \quad (8)$$

where we defined $\omega_0 \equiv \frac{qB_0}{m}$ and $\omega_z^2 \equiv \frac{2qV_0}{md^2}$. Using equation (2) gives us three equations of motion, one for each spatial component, which are

$$\ddot{x} - \omega_0\dot{y} - \frac{1}{2}\omega_z^2x = 0, \quad (9a)$$

$$\ddot{y} + \omega_0\dot{x} - \frac{1}{2}\omega_z^2y = 0, \quad (9b)$$

$$\ddot{z} + \omega_z^2z = 0. \quad (9c)$$

The general solution of eq. (9c) is

$$z(t) = c_1 \cos(\omega_z t) + c_2 \sin(\omega_z t), \quad (10)$$

where $c_1, c_2 \in \mathbb{R}$ are determined by initial conditions.

Equations (9a) and (9b) are coupled, so we introduce a complex function $f(t) = x(t) + iy(t)$ to write them as a single differential equation. Multiplying equation (9b) with i and adding it to equation (9a) we obtain the following:

$$\begin{aligned} \ddot{x} + i\ddot{y} + \omega_0(i\dot{x} - \dot{y}) - \frac{1}{2}\omega_z^2(x + iy) &= 0, \\ (\ddot{x} + i\ddot{y}) + i\omega_0(\dot{x} + iy) - \frac{1}{2}\omega_z^2(x + iy) &= 0. \end{aligned} \quad (11)$$

We recognize the first and second parentheses as \ddot{f} and \dot{f} , respectively. The differential equation for $f(t)$ is

$$\ddot{f} + i\omega_0\dot{f} - \frac{1}{2}\omega_z^2 f = 0, \quad (12)$$

which has the general solution

$$f(t) = A_+ e^{-i(\omega_+ t + \phi_+)} + A_- e^{-i(\omega_- t + \phi_-)}, \quad (13)$$

where ϕ_+ and ϕ_- are constant phases, A_+ and A_- are positive amplitudes and

$$\omega_{\pm} = \frac{\omega_0 \pm \sqrt{\omega_0^2 - 2\omega_z^2}}{2}. \quad (14)$$

The physical coordinates are then $x(t) = \text{Re } f(t)$ and $y(t) = \text{Im } f(t)$. The ω_+ is the modified cyclotron frequency and the ω_- is the magnetron frequency, which we will discuss in section V.

In order to have a bounded solution for the particle in the (x, y) -plane, we must have $|f(t)| < \infty$ as $t \rightarrow \infty$. We see from equation (13) that this condition is fulfilled if $\omega_{\pm} \in \mathbb{R}$. From equation (14), this translates to the following constraint on ω_0 and ω_z :

$$\begin{aligned} \omega_0^2 &\geq 2\omega_z^2, \\ \frac{q}{m} &\geq \frac{4V_0}{(B_0 d)^2}, \end{aligned} \quad (15)$$

where we used the definitions of ω_0 and ω_z to get a constraint relating the particle properties with the Penning trap parameters. This allows us to choose appropriate parameters for our Penning trap, depending on the mass of the particle we consider.

Knowing that the particles are bound in the (x, y) -plane, we want to consider the upper and lower bounds, R_+ and R_- respectively, on the particle's distance from the origin. With $f(t)$ being a complex function, its magnitude is found by $|f(t)| = \sqrt{f(t)f^*(t)}$. Defining $\alpha_{\pm} \equiv \omega_{\pm} t + \phi_{\pm}$ to simplify the expressions, we get

$$|f^2(t)| = A_+^2 + A_-^2 + A_+ A_- \left(e^{i(\alpha_+ - \alpha_-)} + e^{-i(\alpha_+ - \alpha_-)} \right). \quad (16)$$

Recognizing the sum of the exponentials as the cosine, $|f(t)|$ becomes

$$|f(t)| = \sqrt{A_+^2 + A_-^2 + 2A_+ A_- \cos(\alpha_+ - \alpha_-)}. \quad (17)$$

The maximum distance from the origin, R_+ , occurs when $\alpha_+ - \alpha_- = 0 \implies \cos 0 = 1$. Similarly, the minimum distance, R_- , is achieved when $\alpha_+ - \alpha_- = \pi \implies \cos \pi = -1$. Equation (17) now gives us simple expression for the two bounds

$$R_+ = \sqrt{(A_+ + A_-)^2} = A_+ + A_-, \quad (18)$$

$$R_- = \sqrt{(A_+ - A_-)^2} = |A_+ - A_-|. \quad (19)$$

C. Multiple particles

So far, we have only considered the presence of a single particle in the Penning trap. With multiple particles simultaneously present in the trap, each particle will now be affected by the Coulomb force from the other particles. The electric field at a point \mathbf{r} due to interactions, $\mathbf{E}_{\text{int}}(\mathbf{r})$, set up by N_p point charges $\{q_1, q_2, \dots, q_{N_p}\}$ at positions $\{\mathbf{r}_1, \mathbf{r}_2, \dots, \mathbf{r}_{N_p}\}$ is given by

$$\mathbf{E}_{\text{int}}(\mathbf{r}) = k_e \sum_{p=1}^{N_p} q_p \frac{\mathbf{r} - \mathbf{r}_p}{|\mathbf{r} - \mathbf{r}_p|^3}, \quad (20)$$

where k_e is Coulomb's constant.

The electric field contributing to the Lorentz force in equation (1) is then $\mathbf{E} = \mathbf{E}_{\text{ext}} + \mathbf{E}_{\text{int}}$, with the external field given by equation (4) as before. Our set of differential equations in equation (9) now get an additional term, and for a particle i , the equations become

$$\ddot{x}_i - \omega_{0,i}\dot{y}_i - \frac{1}{2}\omega_{z,i}^2 x_i - k_e \frac{q_i}{m_i} \sum_{j \neq i} q_j \frac{x_i - x_j}{|\mathbf{r}_i - \mathbf{r}_j|^3} = 0, \quad (21a)$$

$$\ddot{y}_i + \omega_{0,i}\dot{x}_i - \frac{1}{2}\omega_{z,i}^2 y_i - k_e \frac{q_i}{m_i} \sum_{j \neq i} q_j \frac{y_i - y_j}{|\mathbf{r}_i - \mathbf{r}_j|^3} = 0, \quad (21b)$$

$$\ddot{z}_i + \omega_{z,i}^2 z_i - k_e \frac{q_i}{m_i} \sum_{j \neq i} q_j \frac{z_i - z_j}{|\mathbf{r}_i - \mathbf{r}_j|^3} = 0. \quad (21c)$$

To simplify the analysis, we will neglect any other contributions affecting the particles inside the trap.

III. METHODS

A. Numerical implementation and integration

We aim to create a program in C++ that simulates a set of N_p particles inside a Penning trap. An object-oriented

code is befitting this task and we present in the following descriptions of the classes **Particle** and **PenningTrap**.

The purpose of **Particle** is to hold the parameters of a particle. We let an object of this class be initialised with a charge q , a mass m , a position $\mathbf{r} = (x, y, z)$ and a velocity $\mathbf{v} = (v_x, v_y, v_z)$. We add functions to update the latter two.

The **PenningTrap**-class imitates the physical system that is the Penning trap, and accepts only input particles of type **Particle**. When filled with $N_p \geq 1$ particle(s), an object of **PenningTrap** is ready to simulate the evolution of the **Particle** object(s) for a given period of time and time step size. Simulation is performed with either a FE or a RK4 numerical scheme, by computing the external electric and magnetic fields according to equations (6) and (7). When interactions are included, the solver includes the electric field contribution according to equation (20).

Numerical integration

The equation of motion (2) is split into two first order ODEs as follows:

$$\begin{aligned}\dot{\mathbf{v}} &= \frac{\mathbf{F}}{m} \\ \dot{\mathbf{r}} &= \mathbf{v}\end{aligned}\tag{22}$$

We then get six discretised equations to solve for each particle at each step in time. We use two different approaches when solving equations (22) numerically. Both methods are single step methods, meaning we advance one time step per iteration. The simpler method, FE [1], is of first order meaning that we advance one time step by considering the gradient at the current time step only. This results in few FLOPs per iteration. Hence, this scheme offers numerical efficiency. The draw back is the accuracy of the resultant solution. For a step size h , the FE scheme has a local truncation error of $\mathcal{O}(h^2)$ which results in a global error $\mathcal{O}(h)$. Since we want h to be small, the global error is large compared to the local error.

The second, more advanced, method is the RK4 methods [1], which is of fourth order. This means that we advance one time step by considering the superposition of four different gradients across a single time step. This results in many FLOPs per iteration. Hence, this scheme is numerically more expensive than the FE scheme. However, it offers a far more accurate solution yielding a local truncation error of $\mathcal{O}(h^5)$ and global error $\mathcal{O}(h^4)$. Again, since h is small, these errors are four orders of magnitudes smaller than those of the FE scheme. As a result, with the RK4 method we are able to obtain a similar accuracy with a much larger step size compared to the FE method.

B. Penning trap parameters and particle properties

For the Penning trap parameters, we choose the following numerical values:

$$d = 500 \mu\text{m}$$

$$V_0 = 25.0 \text{ mV}$$

$$B_0 = 1.00 \text{ T}$$

We convert all quantities to the following set of base units:

$$\text{Unit-length} = \text{one micrometre} = 1 \mu\text{m}$$

$$\text{Unit-time} = \text{one microsecond} = 1 \mu\text{s}$$

$$\text{Unit-mass} = \text{one atomic mass unit} = 1 \text{ u}$$

$$\text{Unit-charge} = \text{one elementary charge} = 1 \text{ e}$$

The particles we consider are Calcium ions (Ca^+) with charge $q = 1 \text{ e}$ and mass $m = 40.078 \text{ u}$. These values ensure that the condition in equation (15) is fulfilled.

C. Initial conditions

For simulations of one or two particles, we use the following initial conditions:

- Particle 1

$$\begin{aligned}\mathbf{r}_0^{(1)} &= (20, 0, 20) \mu\text{m} \\ \mathbf{v}_0^{(1)} &= (0, 25, 0) \mu\text{m}/\mu\text{s}\end{aligned}$$

- Particle 2

$$\begin{aligned}\mathbf{r}_0^{(2)} &= (25, 25, 0) \mu\text{m} \\ \mathbf{v}_0^{(2)} &= (0, 40, 5) \mu\text{m}/\mu\text{s}\end{aligned}$$

D. Particle simulations

We begin by simulating a single particle, using the initial conditions for Particle 1 in section III C. We compare the resulting axial motion obtained from FE and RK4 with the analytical solution in equation (10) which has the specific solution

$$z(t) = z_0 \cos(\omega_z t),\tag{23}$$

where $z_0 = 20 \mu\text{m}$. We simulate over a duration of $T_1 = 50 \mu\text{s}$, using $n_1 = 4000$ steps.

To study the accuracy of the two algorithms, we compute the size of the relative error of the two algorithms as a function of time for a duration of T_1 . To study the step size dependency, we do this for four different number of time steps:

$$n_1 = 4000$$

$$n_2 = 8000$$

$$n_3 = 16000$$

$$n_4 = 32000$$

The size of the relative error is given by

$$\Delta_{\text{rel},k} = \frac{|\mathbf{r}_{\text{exact}} - \mathbf{r}_k|}{|\mathbf{r}_{\text{exact}}|}, \quad (24)$$

where $\mathbf{r}_{\text{exact}}$ is the analytical solution. For the movement in the (x, y) -plane, the specific solution for $f(t)$ is given by equation (13) with

$$\begin{aligned} A_+ &= \frac{v_0 + \omega_- x_0}{\omega_- - \omega_+}, & A_- &= -\frac{v_0 + \omega_+ x_0}{\omega_- - \omega_+}, \\ \phi_+ &= 0, & \phi_- &= 0, \end{aligned} \quad (25)$$

where $v_0 = \dot{y}(0) = 25 \mu\text{m}/\mu\text{s}$ and $x_0 = 20 \mu\text{m}$. $z(t)$ is given by equation (23).

Using the results of the estimated errors, we will estimate the error convergence rate, r_{err} , for our two algorithms

$$r_{\text{err}} = \frac{1}{3} \sum_{k=2}^4 \frac{\log(\Delta_{\text{max},k}/\Delta_{\text{max},k-1})}{\log(h_k/h_{k-1})}, \quad (26)$$

where $h_k = T_1/n_k$ is the step size and

$$\Delta_{\text{max},k} = \max_i |\mathbf{r}_{i,\text{exact}} - \mathbf{r}_i| \quad (27)$$

is the maximum size of the absolute error with n_k time steps. The global truncation error of our two methods have different h dependence, as discussed in section III A. r_{err} provides a simple estimated measure of how fast the two methods converge to the true value when we decrease h .

Having studied the accuracy of our solver, we proceed by studying two particles in the Penning trap with the initial conditions specified in section III C. For $n_2 = 8000$ timesteps we simulate the two particles over a duration of T_1 , both with and without interactions, using the RK4 method. In both cases, we will study the motion of the two particles in the (x, y) -plane, their trajectories in the (x, v_x) -plane and the (z, v_z) -plane and a 3D plot showing their trajectories in (x, y, z) space.

E. Many particles - Resonance

Now that the basics of our Penning trap is complete, we explore resonance features of our trap when we have a large number of particles in the trap. To do this, we subject the system to a time-dependent electromagnetic field by making the replacement

$$V_0 \rightarrow V_0(1 + f \cos(\omega_V t)), \quad (28)$$

where f is a constant amplitude and ω_V is the angular frequency of the time-dependent potential. Using this

potential, we will consider $N_p = 100$ particles with standard normal distribution for their initial positions and velocities. The magnitude of each particle's initial position and velocity vector is then scaled by a factor $d/10$. To find potential resonance frequencies, we will plot the fraction of particles that are left in the trap after a duration of $T_2 = 500 \mu\text{s}$ ¹ as a function of applied frequency $\omega_V \in [0.2, 2.5] \text{ MHz}$. For this broad frequency range we use a step size of 0.02 MHz for the applied frequencies and switch off the interactions between the particles. We plot the result for the three amplitudes $f = 0.1, 0.4, 0.7$, using $n = 80000$ time steps. Using only the RK4 scheme, we perform two sorts of frequency scans:

- (i) **Broad-band resonance search:** Run many simulations with interactions switched *off* for a broad range of frequencies, but with equal magnitude of the perturbation. Log the number of particles remaining in the trap after each simulation.
- (ii) **Narrow-band resonance search:** Run several simulations with interactions turned *on* for a narrow range of frequencies. The band is determined using the result of (i) to locate a small range of response frequencies. Repeat with interactions turned *off* for comparison. Write down the number of particles trapped at T_2 .

IV. RESULTS

A. Single particle

We run the first simulation as explained in section III D. In Figure 2 we plot the z -component of the position as function of time. The solutions are found both using the FE and RK4 schemes, shown in red and blue respectively. The analytical solution, found from equation (23) is shown with green in the figure.

Since both FE and RK4 are approximations of the analytical solution we expect them to have a relative error compared with it. We find this error from equation (24) for n_k with $k = 1, 2, 3, 4$. The results are shown in Figures 3 and 4.

We compute the convergence rate according to equation (26) and find that $r_{\text{err}} \simeq 3.9$ for RK4 and that $r_{\text{err}} \simeq 1.4$ for FE. This is close to our expected convergence rate, which is the order of the numerical scheme, 4 and 1 for the RK4 and FE methods respectively.

B. Two particles

We simulate Particle 1 and Particle 2 for a duration of T_1 , using RK4 with n_2 time steps both with and and

¹ Strictly speaking, some simulations are stopped before this due to the trap being emptied.

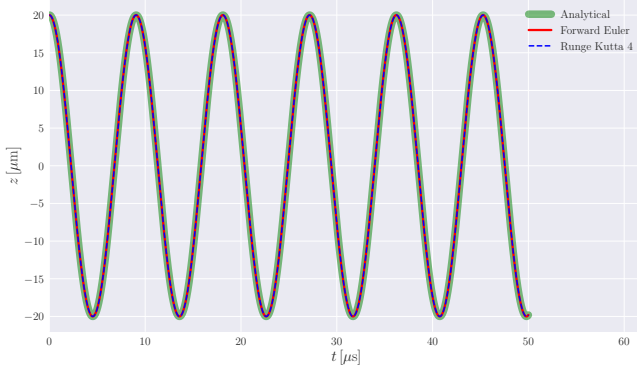


FIG. 2. Movement in the z -plane for a single particle, simulation for $T_1 = 50 \mu\text{s}$ with $n_1 = 4000$ time steps. The analytical solution from equation (10) is plotted in green, and the integrated solutions using the FE and RK4 scheme is shown in red and blue respectively. Initial conditions are those of Particle 1, given in III C.

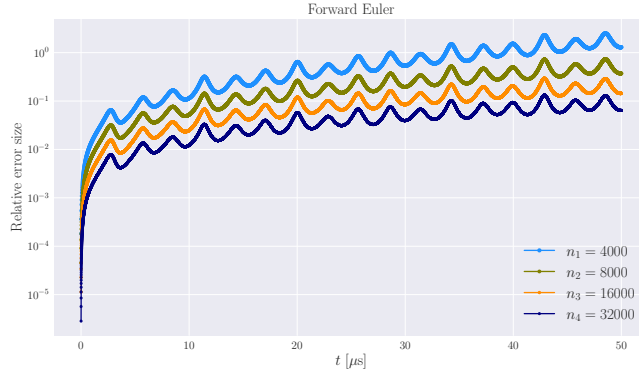


FIG. 3. Relative error of the FE scheme, simulated for $T_1 = 50 \mu\text{s}$, for a different amount of steps n_k with $k = 1, 2, 3, 4$ as indicated in the figure legend. Pay attention to the logarithmic y -axis.

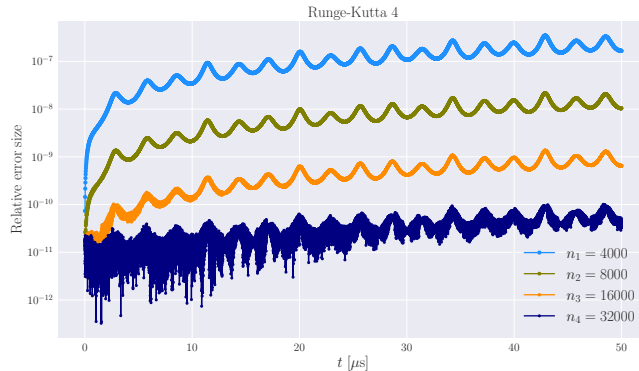


FIG. 4. Relative error of the RK4 scheme, simulated for $T_1 = 50 \mu\text{s}$, for a different amount of steps n_k with $k = 1, 2, 3, 4$ as indicated in the figure legend. Pay attention to the logarithmic y -axis.

without Coulomb interactions. For the three figures soon to be mentioned, Particle 1 is shown in blue, Particle 2 in red, initial conditions are as specified in section III C and the start and end point of their trajectories are indicated with a cross and a star respectively. Figure 5 show the movement of the two particles in the (x, y) -plane. The left panel when we have no Coulomb interaction, and the right panel when they interact.

Figure 6 show the phase plots of the two particles along the x -axis, and Figure 7 along the z -axis.

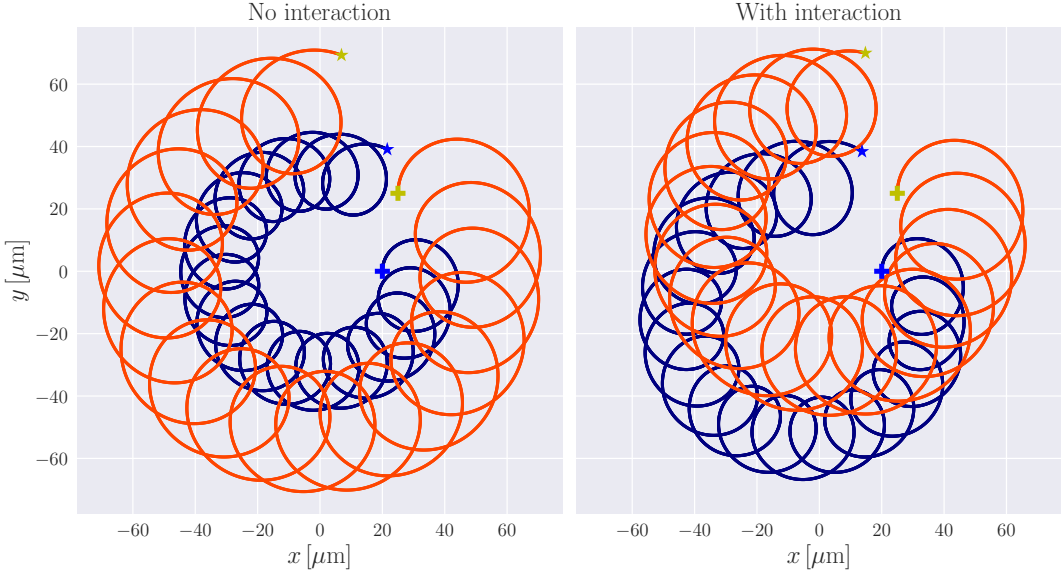


FIG. 5. Movement of two particles in the (x, y) -plane simulated for $T_1 = 50 \mu\text{s}$. The left panel shows their behaviour without interactions and the right panel with. We have used the RK4 scheme to obtain these trajectories. Particle 1 is shown in blue, and Particle 2 in red. Both panels use the same initial conditions as specified in section III C. The starting points of their trajectories are indicated with a cross, their ending points with a star.

C. Many particles

Three broad-band scans are performed, one for each of the amplitudes $f = 0.1, 0.4$, and 0.7 . In particular, we run 300 simulations where we use the same amplitude f and for each run, apply a different frequency $\omega_V \in [0.2, 2.5] \text{ MHz}$. We reused the time step size from section IV B. The fraction of particles remaining is presented in Figure 9 as a function of applied frequency.

For the next step, we choose the smallest amplitude and the middlemost response in Figure 9, i.e. $f = 0.1$ and $\omega_V \in [1.35, 1.45] \text{ MHz}$. We run 50 simulations, each with slightly different applied frequency, for which interaction forces are included. The number of steps is reduced to 20 000 in this case, corresponding to a step size $2T_1/n_1$ (twice that of the first simulation in section IV A). We repeat for interactions switched off. Figure 10 shows N_{trapped}/N_p as a function of ω_V in both cases.

V. DISCUSSION

A. Single particle

We provide the movement in the z -direction in Figure 2 as some sort of test to see whether the numerical integrations methods work or not. Hence, we use the fewest number of time steps, n_1 in order to reveal the largest potential errors. From the figure they seem to

overlap perfectly, however there is reason to think the errors in the calculated solutions grow with time. This is indeed the case, as the error for the small duration T_1 is not visible due to the thickness of plotted lines and the scale of the plot. Although not shown here, if we were to zoom in on the graphs at a late time they do not overlap, i.e. indicating that there is an error although hard to spot. Nevertheless, the calculated solution seems to fit the analytical quite well, but we are still interested in quantifying the error, which we expect to be smaller if we increase the number of time steps.

Using the analytical solution as reference, the relative error as found from equation (24) is shown in Figure 3 for the FE scheme and in Figure 4 for the RK4 scheme. Here, all four time steps n_k with $k = 1, 2, 3, 4$ are included. The increase in error for both plots as we increase the number of time steps seems to follow the order of the global error for each scheme. This also becomes apparent when considering the actual relative error in the plots (y -axis values), and the magnitudinal decrease in error when we increase the number of time steps. The latter is significantly more apparent for the RK4 scheme, which is to be expected as the global error should go as $\mathcal{O}(h^4)$, rather than $\mathcal{O}(h)$ for the FE scheme. This coincides with the values of r_{err} we previously estimated. The RK4 method converges much faster towards the actual solution. Thus, increasing the number of time steps results in a much larger change in relative error than for the FE method. The apparent large error variations of the graphs in Figure 4 can be explained by the small numerical values of

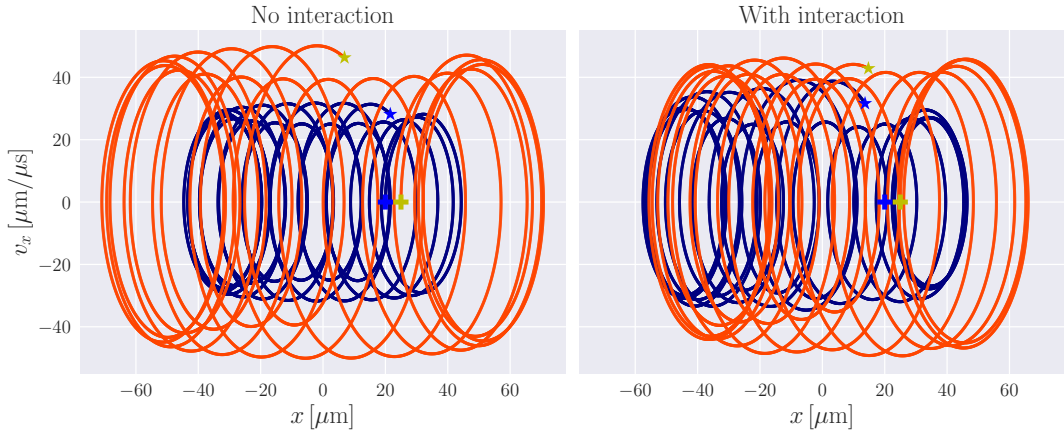


FIG. 6. Phase plots along the x -axis for two different particles simulated for $T_1 = 50 \mu\text{s}$. The left panel show their behaviour without interactions and the right panel with. Particle 1 is shown in blue, and Particle 2 in red. Both panels use the same initial conditions as specified in section III C. The starting points of their trajectories are indicated with a cross, their ending points with a star.

the relative error, and the fact that we use a logarithmic y -axis, which emphasize the variation for small errors (broad fuzzy looking graph for n_4).

B. Two particles

In the simulations where we use two noninteracting particles, the trajectories are easily predictable as they correspond to two single-particle cases. The movement in the (x, y) -plane in this case is shown in the left panel of Figure 5, whereas the interacting particles' orbital motion is presented in the right panel. The noninteracting particles move in the radial plane according to two modes, one with frequency ω_+ orbiting around the magnetic field lines and another with frequency ω_- that gives rise to the slow orbit around the centre of the trap. The former is called the modified cyclotron motion and the latter is the magnetron motion. The interacting particles show similar tendencies, but the orbiting magnetron motion is shifted a bit in the radial plane due to the particles' repulsion between each other. The radii of said orbits tend to increase in both cases, although not very obviously from the figure for Particle 2. The other mode, the modified cyclotron motion, is affected oppositely by the interaction forces for the two particles. The orbit Particle 1 has around the magnetic field lines generally seems to increase in radius where the reciprocal radius for Particle 2 decreases, and vice versa.

We present the phase plots in the x -plane in Figure 6, in which the left panel indicates the periodic motion in

one of the radial directions when there are no interaction forces present. The elliptical phases have for both particles a more or less constant size, but move around in the phase space as each particle moves along the x -axis. The former phenomena arise from the modified cyclotron motion, whereas the latter is due to the slow magnetron motion. The same nature is seen for the other radial direction, although we do not present the phase plot in the y -plane here. Coulomb interactions seem to especially affect the slow orbital motion around the centre as the periodicity of the ellipses in the phase space is quickly reduced. However, after a while, the phase space ellipses change significantly in size as well. This is consistent with what we see in Figure 5.

The left panel in Figure 7 tells us simply that the axial motion is a harmonic oscillator. In the right panel of the same figure, we see how the repulsion between them affects this oscillating movement. The interacting particles are moving up and down along the z -axis with varying ranges and frequencies. We notice that the particles are still confined to a small length in the axial direction.

The three-dimensional trajectories in Figure 8 substantiate the discussion of periodicity and quasiperiodicity for noninteracting and interacting particles, respectively. In summary, introducing Coulomb forces gives rise to more chaotic and possibly unstable motions, for which the original magnetron motion seems especially prone to instabilities.

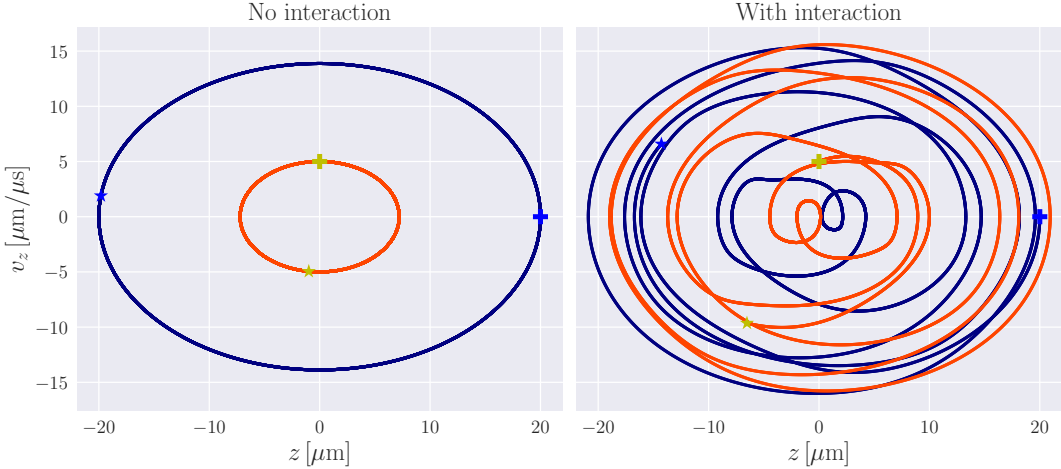


FIG. 7. Phase plots along the z -axis for two different particles simulated for $T_1 = 50 \mu\text{s}$. The left panel show their behaviour without interactions and the right panel with. Particle 1 is shown in blue, and Particle 2 in red. Both panels use the same initial conditions as specified in section III C. The starting points of their trajectories are indicated with a cross, their ending points with a star.

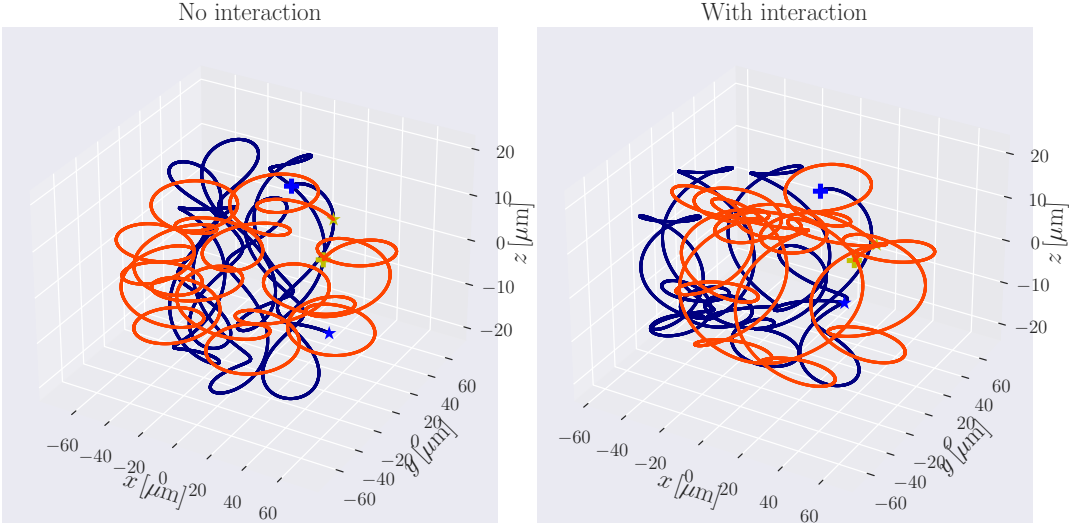


FIG. 8. The trajectory of Particle 1 (blue) and Particle 2 (red) in the Penning trap for $T_1 = 50 \mu\text{s}$. The left panel show their behaviour without interactions and the right panel with. The starting points of their trajectories are indicated with a cross, their ending points with a star.

C. Resonance

From Figure 9 we see how an oscillating electric potential gives rise to the *escapement* of particles in the Penning trap. For some bands of applied frequencies, all

particles have escaped before the simulation has ended. Increasing the amplitude of the perturbation has two main effects. The first effect is that for resonance occurring near a particular frequency, a broader range of neighbouring frequencies also produce resonance effects.

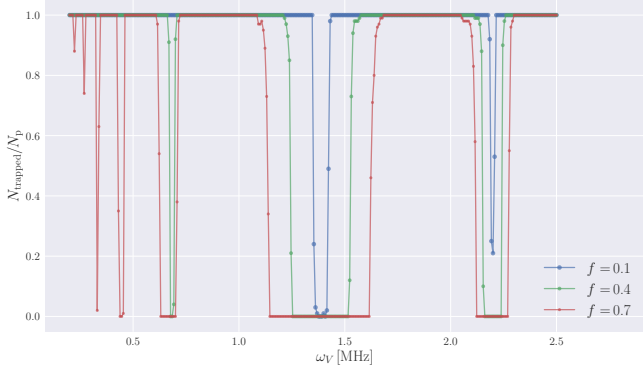


FIG. 9. Fraction of particles that are still trapped by the Penning trap, N_{trapped} , after $T_2 = 500 \mu\text{s}$, as function of the applied frequency $\omega_V \in [0.2, 2.5]$ MHz, for different amplitudes $f \in \{0.1, 0.4, 0.7\}$, without considering particle interactions. All graphs are resulting from simulations using $n = 80000$ time steps.

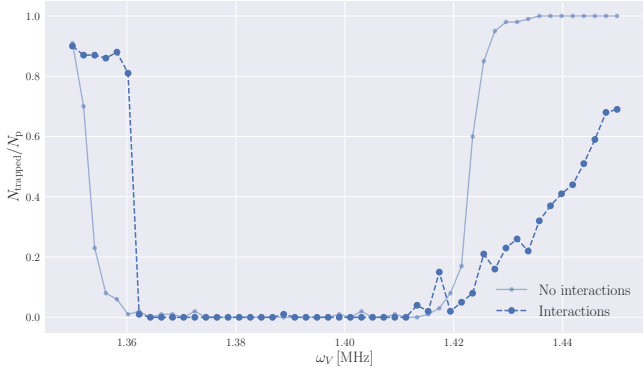


FIG. 10. Fraction of particles that are still trapped by the Penning trap, N_{trapped} , after $T_2 = 500 \mu\text{s}$, as function of selected applied resonance frequencies $\omega_V \in [1.35, 1.45]$ MHz, with amplitude $f = 0.1$, both with and without particle interactions. Both graphs are resulting from simulations using $n = 20000$ time steps.

This is apparent for $\omega_V \sim 1.4 \pm \Delta\omega_V$ MHz, where resonance is evident for $\Delta\omega_V \sim 0.2$ MHz when $f = 0.7$. For $f = 0.1$, Figure 10 indicates that $\Delta\omega_V \lesssim 0.05$ MHz in comparison. The other main effect is that the fraction of particles escaping at certain frequencies increases. At $\omega_V \sim 2.2$ MHz we see from Figure 9 that $f = 0.1$ and $f = 0.7$ yields $N_{\text{trapped}}/N_p \sim 0.2$ and $N_{\text{trapped}}/N_p = 0$, respectively. At $\omega_V \sim 0.7$ MHz we see that $f = 0.1$ is insufficient for particles to escape, and for $\omega_V < 0.5$ MHz particles escape when $f = 0.7$ only.

When it comes to the frequency dependence of resonance behaviour there may be numerous reasons why the particles in the Penning trap is particularly vulnerable to some specific frequencies. We will only present some of the plausible explanations. A thorough discussion of resonance phenomena is beyond the scope of this report.

The particles' motion in the Penning trap have some

quasi-periodic features. For a single particle, we know that the axial motion is governed by oscillations with a frequency of ω_z . For a harmonic oscillator, the resonance frequency due to an applied oscillating force will be close its eigenfrequency. Our perturbation alters the differential equation for z , however, since the applied oscillation is multiplied with z in equation (9c). Nonetheless, it's reasonable to assume that $\omega_V \sim \omega_z$ induces resonance, which would correspond to the drops at $\omega_V \sim 0.7$ MHz in figure 9. Similarly for the movement in the (x, y) -plane, we may expect that certain values of ω_V expressed as different combinations of ω_+ , ω_- and ω_z result in the particles being pushed further out in the plane, causing them to eventually escape the trap. ω_+ and ω_- governed the periodic motions in the (x, y) -plane for the static potential. Although these frequencies are altered by the time-dependent potential, we find it reasonable to assume that a somewhat similar quasi-periodic behaviour may occur in the time-dependent potential trap, with some corresponding new frequency values. It is then likely that for ω_V close to these new frequency values, resonance will occur.

Without any further investigations, we can only speculate why the resonance frequencies have their particular values. One major drawback of our analysis is that we only sampled $N_p = 100$ random particles once. The resonance frequencies we see in Figure 9 are therefore not necessarily the true resonance frequencies, as other initial particle configurations will be affected differently by the applied frequencies in question. Computing the resulting average of multiple initial configurations would reduce the statistical uncertainties, and is a natural starting point for further analysis. We can then estimate the true resonance frequencies with higher accuracy. One possible way of determining what actually sets the value of the resonance frequencies, is to repeat the forementioned analysis several times, using different parameters for the Penning trap and different particles each time. If resonance occurs at frequencies that are different combinations of ω_+ , ω_- and ω_z , one may study whether the numerically estimated resonance frequencies for different setups concur with analytical expressions. The drawback of this method is that running multiple scans to explore resonance frequencies is computationally expensive, even for a single Penning trap. Repeating this for many different trap setups will not necessarily be the most effective approach. One method of gaining more insight into which parameters govern resonance at different frequencies, is to consider the trap limits in (x, y, z) -space, and count the number of particles escaping in different directions as a function of applied frequencies. The positions at which particles escaped are unknown to us from our method of choice.

Without interactions, Figure 9 indicates that there are sharp transitions in applied frequencies where either all particles escape or they all remain trapped. This may be a consequence of considering one sample only for our analysis, and could be resolved with multiple samples.

Another possible reason for this, is that our step size of ω_V is too large. In Figure 10 we see that a higher frequency resolution do yield less sharp transitions, but not by a significant amount.

When particle interactions are included, we see from Figure 10 that many particles continues to escape at the high frequency end, where we previously had no particles escaping. This is likely due to repulsive Coulomb forces pushing some particles further out from the origin. A surprising feature is that for the low frequency end, a larger fraction of the interacting particles remain trapped at frequencies where the non-interacting particles escapes. The reason for this is not apparent, and additional sampling should be considered to determine if this effect is statistically significant.

The time step size is relatively large for the simulations with Coulomb interactions turned on. This could be a source of instabilities, but as these simulations are computationally expensive, we do not explore potential consequences of this any further.

VI. CONCLUSION

We conclude that our implementation and testing of both the FE ad RK4 scheme is correct since the solutions appear accurate in Figure 2, and the errors from Figures 3 and 4 behave as we expect them to. We also conclude that the convergence rates found for both methods are satisfying as they resemble their numerical order.

For the two particle simulation, allowing them to interact pushes the particles further away from each other, while both still show periodic behaviour. This is the physical solution as we are not able to switch off these interaction in a physical Penning trap. The effect we see when including the Coulomb forces is a more chaotic

behaviour.

Introducing a time-dependent perturbation to the electric potential does indeed give rise to resonance phenomena, as certain resonance frequencies empty the trap completely by pushing all particles out of it. We find these frequencies to be bands whose widths are determined by the applied amplitudes f and centred around $\omega_V \in \{0.7, 1.4, 2.2\}$. Without particle interactions, the majority of applied frequencies seem to either leave all the particles contained within the trap, or eject them all. When we include Coulomb interactions, there seems to be slight middle ground where some have escaped and some are still trapped. Thus particles interactions seem to sometimes work against the resonance frequencies, preventing some particles from escaping the trap as quickly as they otherwise would. However, our results were obtained by considering one sample of random particles in the trap. To obtain more accurate results multiple sampling would be the next natural step to further investigate the resonance behaviour of the Penning trap.

We also question the validity of these results due to the larger time step used in order to speed to computation time. A natural extension of this would be to run the simulation for smaller time steps, although this will increase computation time. Another approach could be to look at a broader range of ω_V values, with smaller step sized. To better understand which frequencies the resonance behaviour is related to, a natural choice of further exploration is to study the spatial distribution of the escaped particles. By also defining the extent of the trap in terms of spatial coordinates, rather than a fixed radius, resonance effects in different directions can be better understood. It would also be interesting to implement the self induced magnetic field set up by moving charges to see whether it has a major impact on our results.

- [1] Atkinson, K. E. (1989). *An Introduction to Numerical Analysis (Second Edition)*, chapter Six, pages 333–443. John Wiley & Sons.
- [2] Dehmelt, H. G. (1989). Hans G. Dehmelt - Biographical.

Retrieved from: <https://www.nobelprize.org/prizes/physics/1989/dehmelt/biographical/> (Oct. 2022).

- [3] Griffiths, D. J. (2017). *Introduction to Electrodynamics (Fourth Edition)*, chapter 3 Potentials, page 118. Cambridge University Press.